

Negative thermal expansion in CuCl: An extended x-ray absorption fine structure study

M. Vaccari, R. Grisenti, and P. Fornasini*

Istituto Nazionale per la Fisica della Materia and Dipartimento di Fisica, Università degli Studi di Trento, I-38050 Povo (Trento), Italy

F. Rocca and A. Sanson

Istituto di Fotonica e Nanotecnologie del CNR, Sezione di Trento, I-38050 Povo (Trento), Italy

(Received 19 January 2007; published 21 May 2007)

Extended x-ray absorption fine structure (EXAFS) has been measured from liquid helium to ambient temperature at the Cu *K* edge of copper chloride (CuCl) to investigate the local origin of negative thermal expansion. A quantitative analysis of the first coordination shell, performed by the cumulant method, reveals that the nearest-neighbor Cu-Cl interatomic distance undergoes a strong positive expansion, contrasting with the much weaker negative expansion of the crystallographic distance between average atomic positions below 100 K. The anisotropy of relative thermal vibrations, monitored by the ratio γ between perpendicular and parallel mean square relative displacements, is considerably high, while the diffraction thermal factors are isotropic. The relative perpendicular vibrations measured by EXAFS are related to the tension mechanism and to the transverse acoustic modes, which are considered responsible for negative thermal expansion in zinc-blende structures.

DOI: [10.1103/PhysRevB.75.184307](https://doi.org/10.1103/PhysRevB.75.184307)

PACS number(s): 61.10.Ht, 65.40.-b, 65.40.De, 87.64.Fb

I. INTRODUCTION

Cuprous chloride CuCl is a highly ionic I-VII semiconductor having the zinc-blende (ZB) structure at ambient temperature and pressure. CuCl has always attracted considerable experimental and theoretical interest because of its unusual physical properties: an ionicity near the critical threshold which divides fourfold from sixfold coordinated structures;¹ anomalously low values of bulk and shear moduli² which give evidence of an approaching elastic instability;³ a large overlapping of the cation and anion electron clouds;^{4,5} large thermal variations of specific heats Debye temperature with respect to the other copper halides;⁶ a very high and anharmonic thermal motion of Cu⁺ ions, revealed by neutron and x-ray diffraction;⁷⁻¹⁰ the presence of several consecutive pressure-induced phase transitions;¹¹ very flat transverse-acoustic (TA) branches along all high symmetry directions;^{12,13} and a double-peak structure of the transverse optic (TO) phonon at the zone center.¹⁴

One of the most interesting features of CuCl is the pronounced negative thermal expansion (NTE) below 100 K.¹⁵ Many tetrahedrally bonded semiconductors with the diamond or zinc-blende structure undergo NTE at very low temperatures (see Ref. 16 and references therein), strength and temperature interval of NTE increasing with ionicity. CuCl exhibits the strongest NTE among tetrahedral semiconductors: the thermal expansion coefficient is minimum at about 30 K ($\alpha_{\min} \sim -8 \times 10^{-6} \text{ K}^{-1}$), and is negative up to 100 K.¹⁷

The recent discovery of materials with framework structures that contract over very large temperature intervals, like ZrW₂O₈ (Ref. 18) and Ag₂O (Ref. 19), has renewed the interest for NTE and stimulated the search for understanding its microscopic mechanisms. The macroscopic thermal expansion is generally considered the result of a competition between a positive contribution due to a bond stretching effect and a negative contribution due to some kind of tension effect.²⁰⁻²² In zinc-blende structures (ZB), the tension effect

prevails only at low temperatures, and is progressively overcome by the stretching effect, giving rise to positive expansion at high temperatures.¹⁶ In some framework structures, like Ag₂O, the tension effect prevails at all temperatures; in others, like the isostructural Cu₂O, the stretching effect becomes stronger at high temperatures, as in zinc blendes.¹⁹

A common feature in materials affected by NTE of vibrational origin seems to be the presence of strong vibrations perpendicular to some interatomic bonds. In framework structures, NTE has been often connected to the presence of low frequency rigid unit modes (RUM), although in some crystals NTE is not accompanied by RUMs, and vice versa;²³ in any case, linear A-B-A links are generally present in framework structures, which favor the tension effect. In ZB structures, no RUM-supporting polyhedral structural units can be identified; besides, all atoms are tetrahedrally coordinated and there are no linear links. In spite of the absence of linear links, in CuCl the low temperature NTE ($\alpha_{\min} \sim -8 \times 10^{-6} \text{ K}^{-1}$) is comparable to that of Ag₂O ($\alpha_{\min} \sim -10.4 \times 10^{-6} \text{ K}^{-1}$) and of ZrW₂O₈ ($\alpha \sim -9.1 \times 10^{-6} \text{ K}^{-1}$), and is much stronger than in Cu₂O ($\alpha_{\min} \sim -2.4 \times 10^{-6} \text{ K}^{-1}$).

The search for a deeper understanding of NTE can greatly benefit from careful comparative studies of both framework and ZB structures, performed by means of a local structural probe, like extended x-ray absorption fine structure (EXAFS).

Bragg diffraction measures the thermal expansion of the cell parameters, which is directly proportional to macroscopic thermal expansion, but can give only partial information on the local behavior. EXAFS is particularly suited for complementing Bragg diffraction, since it is sensitive to correlation of atomic vibrations, and can give unique insights on the local thermal behavior of materials. EXAFS measures the thermal expansion of the average distance between nearest neighbors (“true bond length”), while Bragg diffraction measures the thermal expansion of the distance between average atomic positions (“apparent bond length”).^{22,24}

Moreover, while Bragg diffraction measures the *absolute* mean square displacements (MSD) of each atom, EXAFS directly measures the mean square *relative* displacements (MSRD) of pairs of atoms parallel to the bond direction. Recently it has been shown that, by comparing the EXAFS and diffraction thermal expansions, it is possible to recover also the MSRD perpendicular to the bond direction.^{24,25} The ratio γ between perpendicular and parallel MSRDs measures the anisotropy of *relative* vibrations, which can be connected to NTE.²⁶ It has to be noticed that for zinc blends, contrary to cuprites, the *absolute* MSDs measured by Bragg diffraction are isotropic.

The potential of EXAFS for studying NTE materials has been up to now little exploited. In an EXAFS study of ZrW_2O_8 , Cao *et al.* focused their attention on the temperature dependencies of the *parallel* MSRDs of different atomic pairs.²⁷ More recently, the possibility of measuring the true bond thermal expansions and the perpendicular MSRDs has been successfully tested on the framework structures Cu_2O and Ag_2O , leading to a more complete picture of the local structure and dynamics of those systems.¹⁹

In this paper, we present an EXAFS study of CuCl , based on measurements performed as a function of temperature from 6 to 300 K, and aimed at investigating the local vibrational origin of the NTE in zinc blends. Previous EXAFS measurements on CuCl ,²⁸ and more generally on copper halides,²⁹ were limited to high temperatures in order to study the transition to the superionic phase.

This paper is organized as follows. Section II summarizes and updates some useful concepts about the treatment of thermal disorder effects in EXAFS spectra. In Sec. III some details on the experiment are given. In Sec. IV the data analysis procedure is described; the two approaches utilized, ratio method and nonlinear fit, are critically compared. In Secs. V and VI the results of the quantitative analysis on the first and outer coordination shells are presented. Secs. VII and VIII are dedicated to discussion and conclusions, respectively.

II. EFFECTS OF THERMAL DISORDER ON EXAFS

The EXAFS signal of one coordination shell samples a one-dimensional distribution $\rho(r)$ of interatomic distances. For systems characterized by a not too strong disorder, the distribution $\rho(r)$ can be parametrized in terms of its cumulants C_n^* .^{30,31} The first three cumulants correspond to mean value, variance, and asymmetry of the distribution, respectively; for systems affected by disorder of only thermal origin, the cumulants can be connected to the local dynamical behavior of the system, i.e., to atomic relative displacements both parallel and perpendicular to the interatomic bond. Higher order cumulants measure further deviations from a Gaussian distribution.

Let us denote by 1 and 2 the absorber and backscatterer atoms, respectively. The average distance $\langle r \rangle = \langle |\mathbf{r}_2 - \mathbf{r}_1| \rangle$ measured by the first EXAFS cumulant is greater than the crystallographic distance between average atomic positions $R_c = |\langle \mathbf{r}_2 \rangle - \langle \mathbf{r}_1 \rangle|$ measured by Bragg diffraction. The difference, of geometrical origin,³² is mainly due to the effect of relative

vibrations perpendicular to the interatomic bond^{24,25,33}

$$C_1^* \equiv \langle r \rangle = R_c + \frac{\langle \Delta u_{\perp}^2 \rangle}{2R_c} + \dots, \quad (1)$$

where $\langle \Delta u_{\perp}^2 \rangle$ is the perpendicular mean square relative displacement, MSRD_{\perp} .

To a very good approximation, the second cumulant corresponds to the parallel mean square relative displacement³⁴

$$C_2^* \equiv \langle (r - \langle r \rangle)^2 \rangle = \langle \Delta u_{\parallel}^2 \rangle + \dots, \quad (2)$$

where $\langle \Delta u_{\parallel}^2 \rangle \equiv \text{MSRD}_{\parallel}$.

In the same way, one finds that the third cumulant is given by

$$C_3^* \equiv \langle (r - \langle r \rangle)^3 \rangle = \langle \Delta u_{\parallel}^3 \rangle + \frac{3}{2R_c} [\langle \Delta u_{\parallel}^2 \Delta u_{\perp}^2 \rangle - \langle \Delta u_{\parallel}^2 \rangle \langle \Delta u_{\perp}^2 \rangle] + \dots. \quad (3)$$

The lowest order term $\langle \Delta u_{\parallel}^3 \rangle$ corresponds to the parallel mean cubic relative displacement (MSRD_{\parallel}). For an ideally harmonic crystal³⁵ it would be zero: the main contribution to the third cumulant thus comes from the anharmonicity of the crystal potential. The second order term on the right-hand side of Eq. (3) is instead nonzero also for a harmonic crystal potential;³¹ the third cumulant is then always different from zero, so that in principle the one-dimensional distribution $\rho(r)$ is never Gaussian.

Both parallel and perpendicular MSRDs can be decomposed into the sum of two un-correlated mean square displacements (MSD) and a displacement correlation function (DCF):

$$\langle \Delta u_{\parallel}^2 \rangle = \langle u_{2\parallel}^2 \rangle + \langle u_{1\parallel}^2 \rangle - 2\langle u_{2\parallel} u_{1\parallel} \rangle, \quad (4a)$$

$$\langle \Delta u_{\perp}^2 \rangle = \langle u_{2\perp}^2 \rangle + \langle u_{1\perp}^2 \rangle - 2\langle \mathbf{u}_{2\perp} \cdot \mathbf{u}_{1\perp} \rangle. \quad (4b)$$

In these equations we have set

$$|\mathbf{u}_i|^2 = u_{i\parallel}^2 + u_{i\perp}^2,$$

$$\mathbf{u}_i \cdot \mathbf{u}_j = u_{i\parallel} u_{j\parallel} + \mathbf{u}_{i\perp} \cdot \mathbf{u}_{j\perp} \quad \text{for } i \neq j.$$

The uncorrelated MSDs $\langle u_{i\parallel}^2 \rangle$ correspond to the parallel thermal factors U_{\parallel} measured by Bragg diffraction. The uncorrelated MSDs $\langle u_{i\perp}^2 \rangle$ are here defined as corresponding to the sum of the perpendicular thermal factors U_{\perp} measured by Bragg diffraction along two independent directions perpendicular to the bond.³² In case of rotational symmetry around the bond direction, $\langle u_{i\perp}^2 \rangle = 2U_{\perp}$.¹⁹ In some cases of high crystal symmetry, harmonic thermal vibrations around the equilibrium positions are isotropic, and the thermal ellipsoids reduce to spheres;³⁶ this is true for CuCl if anharmonic effects are neglected. We then have

$$\langle u_{i\parallel}^2 \rangle = \langle u_i^2 \rangle / 3, \quad (5a)$$

$$\langle u_{i\perp}^2 \rangle = 2\langle u_{i\parallel}^2 \rangle, \quad (5b)$$

where $u_i^2 \equiv |\mathbf{u}_i|^2$. The ratio γ between perpendicular and parallel MSRDs assumes then a simple expression:

$$\gamma = \frac{\langle \Delta u_{\perp}^2 \rangle}{\langle \Delta u_{\parallel}^2 \rangle} = 2 + \frac{4}{\langle \Delta u_{\parallel}^2 \rangle} \left\{ \langle u_{2\parallel} u_{1\parallel} \rangle - \frac{1}{2} \langle \mathbf{u}_{2\perp} \cdot \mathbf{u}_{1\perp} \rangle \right\}. \quad (6)$$

The greater is γ , the larger is the correlation of the relative atomic motion parallel to the interatomic bond with respect to the average correlation in any two directions perpendicular to the bond. An alternative expression of the ratio γ in terms of the Cartesian components of atomic thermal displacements has been given in Ref. 37 for the diamond structure. Here we express the correlation of atomic motion referring to the *parallel* direction and to the *perpendicular* plane with respect to the interatomic bond: Eq. (6) has the advantage of being independent of a particular choice of coordinates or a given crystal structure. In the ideal case of a perfectly isotropic relative motion, γ would be equal to 2. Actually, even for crystals with isotropic *absolute* thermal motion, EXAFS monitors an anisotropy in the *relative* thermal motion: The ratio γ has been experimentally found greater than 2 for both copper²⁴ and germanium.²⁵

III. EXPERIMENT

A homogeneous sample was prepared by depositing a CuCl powder (99.995% pure, purchased from Aldrich Chemical Co.) on a polytetrafluoroethylene membrane. Appropriate quantities of CuCl were deposited (~ 9 mg/cm²) so as to have a sample thickness of about 20 μ m, which provided an edge jump $\mu x \sim 1.1$ at the Cu *K* edge. The purity of the zinc-blende structure of the sample had been checked by a Rietveld analysis of powder x-ray diffraction spectra.

The EXAFS experiment has been made with synchrotron radiation in transmission mode at the BM08 (Gilda) beamline of ESRF (European Synchrotron Radiation Facility) in Grenoble (France). Electron energy and average current were 6 GeV and 190 mA, respectively. The x-ray beam was monochromatized by two parallel silicon crystals with flat (311) reflecting faces, detuned to reduce the harmonics influence. The incident beam size on the sample was about 4×1 mm². The incoming and outgoing photon fluxes were measured by two ionization chambers filled with argon (at pressures 100 and 400 mbar, respectively).

Temperature dependent EXAFS measurements on CuCl have been performed at the *K* edge of copper from 6 to 300 K. The sample temperature was changed by steps varying from 10 K at low temperatures (below 100 K) to 50 K at higher temperatures. The sample was immersed in a helium gas atmosphere within a liquid helium cryostat. The temperature control was achieved through an electric heater, controlled by a feedback loop. Thermal stabilization was guaranteed within ± 1 K. The acquisition time was 5 s/point. Two or three spectra were collected at each temperature to allow an evaluation of experimental uncertainty.

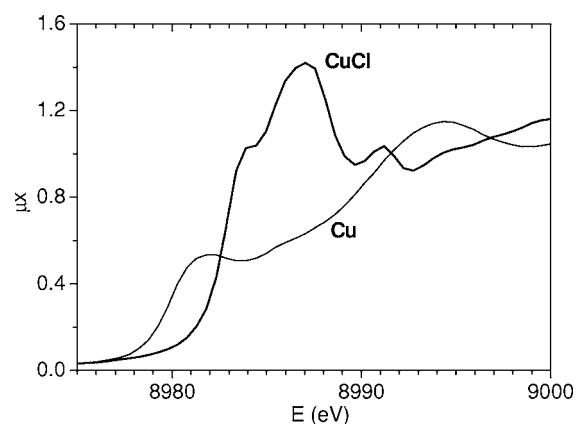


FIG. 1. *K* absorption edges of CuCl (thick line) and Cu (thin line).

For energy-scale calibration purposes, the absorption of a copper reference foil placed past the second ionization chamber, and maintained at room temperature, was contemporarily measured. The two *K* edges of copper and CuCl are compared in Fig. 1. The edge position, here defined as the inflection point of lowest energy³⁸ and measured by the first maximum of the first derivative, was 3.10 ± 0.03 eV higher in CuCl than in Cu.

IV. DATA ANALYSIS

A. Extraction of the EXAFS signal

At the beginning of the analysis, the edges of all spectra were aligned to within 0.1 eV in order to guarantee a resolution of the order of 0.001 \AA in the evaluation of relative distances. The EXAFS signal was obtained as $\chi(k) = (\mu - \mu_0) / \mu_1$, where μ is the experimental absorption coefficient, μ_0 is a spline polynomial best fitting the average behavior of μ (Fig. 2), and μ_1 is a Victoreen-type function with absolute values normalized to the absorption jump of the spectra. The

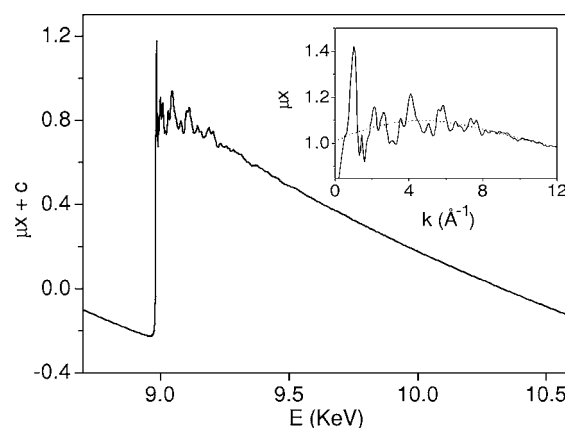


FIG. 2. X-ray absorption spectrum at copper *K* edge of CuCl measured at 6 K. In the inset the absorption coefficient (continuous line) and the smooth background μ_0 (dotted line) are shown in correspondence of the photoelectron wave-number interval $k = 0-12$ \AA^{-1} .

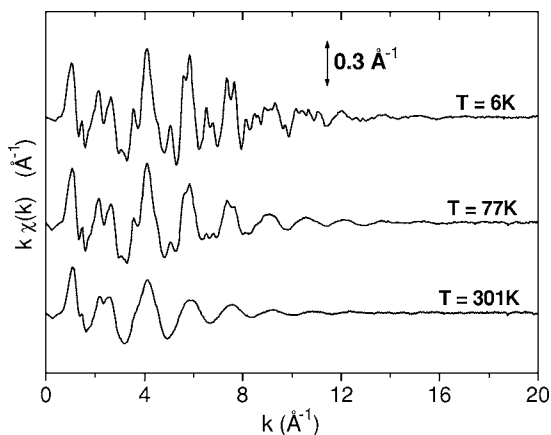


FIG. 3. Normalized EXAFS oscillations $k\chi(k)$ in CuCl at 6, 77, and 301 K.

k -weighted EXAFS function $k\chi(k)$ at selected temperatures is shown in Fig. 3.

The modulus and imaginary part of Fourier transforms at selected temperatures are shown in Fig. 4. The peak centered at about 2 Å, due only to the first-shell contribution, is well-isolated at all temperatures. The structure between about 2.7 and 4.6 Å, formed by two peaks which are distinguishable at 6 K but progressively merge and disappear when temperature increases, is due to the superposition of single scattering (SS) contributions from second and third shells as well as of important noncollinear multiple scattering (MS) contributions.

Two different procedures were considered to obtain quantitative information. The first procedure was utilized only for the first coordination shell, whose contribution can be neatly isolated and where MS effects are absent. It consisted of a separate analysis of phase and amplitude of the filtered EXAFS signal through the ratio method,^{30,39} taking the lowest temperature spectra as reference for backscattering amplitudes, phase shifts, and inelastic terms (assumed to be temperature independent). In the second procedure, backscattering amplitudes, phase shifts, and inelastic terms were

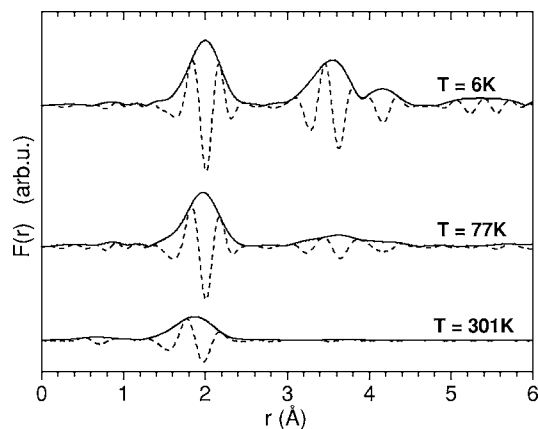


FIG. 4. Modulus (continuous line) and imaginary part (dashed line) of the Fourier transform of the weighted EXAFS signal $k^3\chi(k)$ at 6, 77, and 301 K. The FT interval was $k=2-14.5$ Å, defined by a 10% Gaussian window.

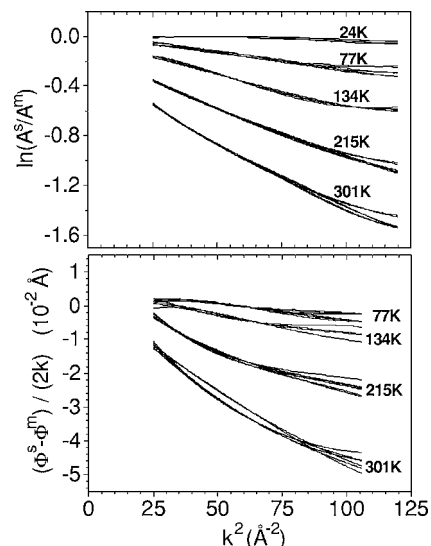


FIG. 5. Examples of analysis by the ratio method at selected temperatures (the reference temperature is taken at 6 K). Upper panel: logarithms of amplitude ratios plotted against k^2 . Lower panel: phase differences (divided by $2k$) plotted against k^2 . For a given temperature, the various lines correspond to different combinations of files and references.

calculated by the FEFF8 code⁴⁰ and a nonlinear best fit to experimental spectra was then performed by the FEFFIT program.⁴¹ For the first-shell analysis, the FEFF8-FEFFIT procedure gave low-temperature results comparable to the ratio method. For the outer shells, it represented the only reasonable way of taking into account both SS and MS contributions.

B. Ratio method

The first-shell contribution was singled out by Fourier back-transform in the range $r=1.3-2.55$ Å with a 5% Hanning window. The filtered EXAFS signal was then compared to the lowest temperature spectra ($T=6$ K). Particular care was taken in comparing only spectra that had undergone exactly the same preliminary steps of analysis: pre-edge and background removal, k -range of Fourier filtering, as well as windows and weights of transform, etc. In particular, the range of Fourier transform was $k=2-17.5$ Å when only low temperature files were compared, and progressively reduced to $k=2-14.5$ Å when higher temperature files were involved. The ratio method directly gives the relative values δC_n of cumulants of an effective distribution³⁰ $P(r,\lambda) = \rho(r)e^{-2r/\lambda}/r^2$. In Fig. 5, logarithms of amplitude ratios and phase differences are plotted against k^2 for selected temperatures. In the amplitudes plot (Fig. 5, upper panel) the linear slope is proportional to the variation of the second cumulant δC_2 (the intercept was fixed to zero, since the coordination number \mathcal{N} is constant); the influence of the fourth cumulant variation δC_4 is also clear as a deviation from linearity. In the phases plot (Fig. 5, lower panel), the vertical intercept is δC_1 while the linear slope is proportional to the third cumulant variation δC_3 ; the deviation from linear behavior indicates the relevance of the fifth cumulant, which actually had

to be taken into account to get meaningful results at the highest temperatures.

Amplitudes and phases were fitted in the suitable range of reliability $k \approx 5-10 \text{ \AA}^{-1}$ (see Fig. 5). At lower and higher k -values, the curves show casual deviations from the expected, regular behavior: this is probably mainly due to spurious effects of Fourier filtering. The uncertainties, expressed as standard deviations of the means, were evaluated by reasonably varying the fitting intervals, as well as cross comparing the results from different files measured at the same temperature with two different references taken at 6 K.

Different analytical and numerical procedures have been proposed for connecting the parameters of the real and effective distributions, limited to the first cumulant^{30,42} or extended to higher order cumulants.³¹ A particularly simple approximate analytical expression has recently been worked out⁴³ to evaluate the cumulants C_n^* of the real distribution $\rho(r)$:

$$C_n^* \sim C_n + 2C_{n+1}(1/C_1 + 1/\lambda) \quad \text{for } n = 1, 2, 3. \quad (7)$$

For $n=1$, Eq. (7) leads to the expression currently used for the first cumulant.³⁰ As far as the second cumulant is concerned, in the case of CuCl, using the experimental values of C_2 and C_3 (see below), Eq. (7) shows that C_2^* is larger than C_2 by about 9% at 300 K, in agreement with numerical simulations.³¹ The difference is not negligible if very accurate results are sought. The electron mean free path $\lambda(k)$ was approximated by a constant value $\lambda \sim 9 \pm 5 \text{ \AA}$ and the uncertainty was propagated up to the final values of δC_n^* .

C. FEFF8-FEFFT method

The input file for the FEFF8 code was generated starting from the atomic coordinates of the ZB structure. This analysis gave physically meaningful results only at temperatures below about 100 K: at higher temperatures, a non-negligible deviation from a regular behavior of cumulants was obtained, probably due to the difficulty in taking into account the fourth cumulant and the impossibility of taking into account the fifth cumulant.

The first shell was fitted in the r -space between 1.3 and 2.55 \AA (see Fig. 6). The number of free parameters was reduced as much as possible. The values of e_0 (mismatch between theoretical and experimental origin of wave-number scales) and S_0^2 (amplitude reduction factor) were left free in a first trial analysis and showed some variation as a function of temperature (typically $e_0=2$ to 3 eV and $S_0^2=0.78-0.81$). Average values were then calculated ($e_0=2.51$ eV and $S_0^2=0.79$) and maintained fixed in a further analysis. The only free parameters were then the first three cumulants, which parametrize the first-shell distribution of distances. The uncertainty of the results was estimated by a least-squares minimization and comparing different files at the same temperature.

The *relative* values of the first three cumulants, referred to the lowest temperature, were all in reasonably good agreement (within the uncertainties) with the results of the ratio method in the range below 100 K. In principle, this analysis procedure should give also the *absolute* values of cumulants;

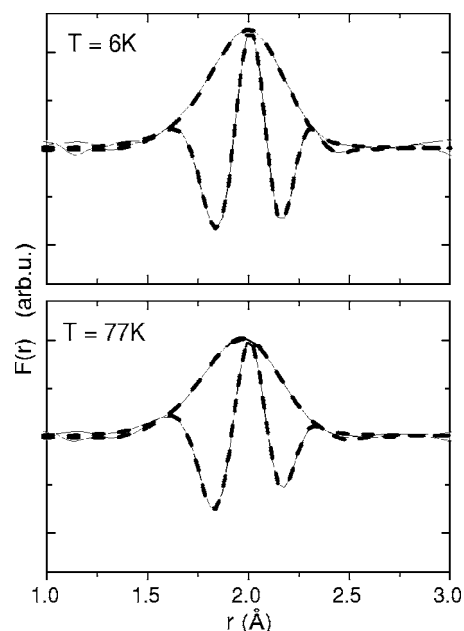


FIG. 6. Modulus and imaginary part of the Fourier transform of the EXAFS signal (continuous lines) and best-fitting signals in the range $r=1.3-2.55 \text{ \AA}$ (dash-dotted lines) at the temperatures of 6 K (upper panel) and 77 K (lower panel).

however, the reliability of absolute values could not be considered accurate enough for studies on negative thermal expansion (for a more detailed discussion, see Ref. 43).

It is interesting to note that the FEFF8 code calculates the mean free path $\lambda(k)$ as a function of k from the imaginary part of the interaction potential, and takes into account its effect through a factor $e^{-2R/\lambda(k)}$, where R is an average distance; the effective distribution becomes $\tilde{P}(r)=\rho(r)/r^2$ and the correction to the first cumulant, Eq. (7) for $n=1$, lacks the $1/\lambda$ term. On the other hand, the ratio method accounts for the instantaneous r -dependence of the whole effective distribution $P(r,\lambda)$, but considers λ as independent of k ; one can, however, show that the errors in phases and amplitudes due to this approximation effectively cancel out in the procedure of comparison of the two files.^{30,31} Anyway, the two procedures based on the FEFF8 and ratio method give thermal expansions in very good agreement in the case of CuCl.⁴³ The same kind of agreement was also found for copper.²⁴

V. RESULTS: FIRST SHELL

A. Thermal expansion

The variation with temperature of the first EXAFS cumulant δC_1^* directly gives the thermal expansion of the Cu-Cl nearest-neighbors bond $\langle r \rangle$, which is compared in Fig. 7 with the corresponding crystallographic expansion δR_c taken from Ref. 15. While R_c shows a negative thermal expansion (NTE) in the range 0–100 K, the average distance $\langle r \rangle$ strongly increases with temperature. This kind of behavior (positive expansion of the first shell average distance and macroscopic NTE) has been found also in other systems like germanium²⁵ and cuprites.¹⁹

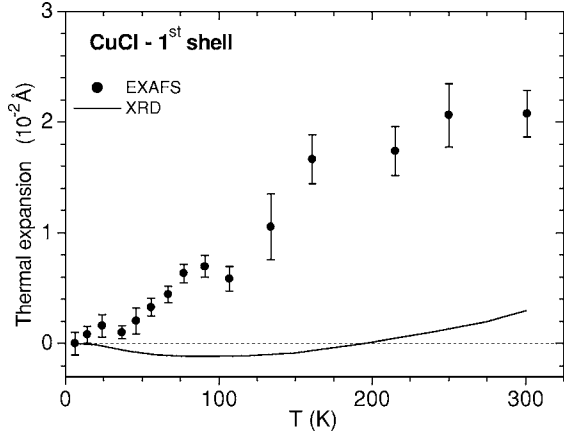


FIG. 7. Thermal expansion of the Cu-Cl nearest neighbors average distance measured by EXAFS (full circles), compared with the corresponding Cu-Cl crystallographic distance (continuous line) taken from Ref. 15.

B. Mean square relative displacements

To a good approximation, the second cumulant corresponds to the parallel mean square relative displacement MSRD_{\parallel} [Eq. (2)]. Absolute values were estimated by fitting the Einstein model for parallel MSRD [Ref. 44] to the experimental data. The correspondence between the experimental points and theoretical model is very good (see Fig. 8). The Einstein frequency is $\nu_E^{\parallel} = (3.93 \pm 0.02)$ THz and the 0 K value is $(5.51 \pm 0.04) \times 10^{-3} \text{ \AA}^2$.

By inverting Eq. (1), the temperature variation of the perpendicular mean square relative displacement (MSRD_{\perp}) was extracted; the behavior was considered reliable enough only in the temperature range below about 100 K. At higher temperatures the inversion of Eq. (1) is probably influenced by the increasing importance of higher order terms. Absolute values for the MSRD_{\perp} were obtained through the Einstein model for perpendicular MSRD (Ref. 44) and are shown in Fig. 8. The Einstein frequency is $\nu_E^{\perp} = (1.66 \pm 0.07)$ THz and the 0 K value is $(2.4 \pm 0.3) \times 10^{-2} \text{ \AA}^2$.

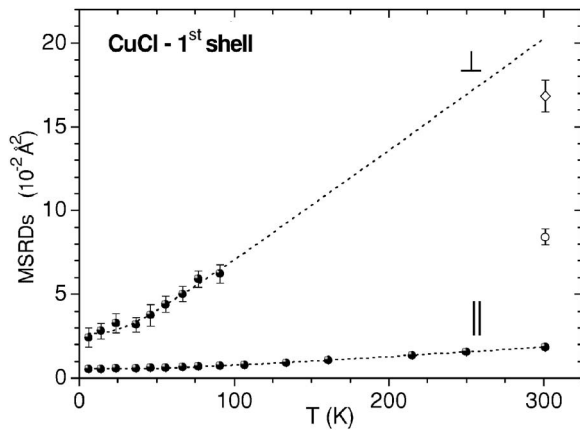


FIG. 8. Parallel and perpendicular MSRD (full circles). The dotted lines are the best-fitting Einstein models. For comparison, the sum of uncorrelated MSDs parallel to bond (open circle) and perpendicular to bond (open diamond) for the Cu-Cl atomic pair are also shown. See the text for discussion.

TABLE I. Parallel and perpendicular MSRDS $\langle \Delta u^2 \rangle$, compared with their lower and upper bounds and with the sum of uncorrelated MSDs for the Cu-Cl atomic pair at room temperature ($T=300$ K). The values are given in 10^{-2} \AA^2 .

	$\langle \Delta u^2 \rangle_{\text{low}}$	$\langle \Delta u^2 \rangle$	$\langle u^2 \rangle_{\text{Cu}} + \langle u^2 \rangle_{\text{Cl}}$	$\langle \Delta u^2 \rangle_{\text{upp}}$
\parallel	0.48 ± 0.01	1.86 ± 0.04	8.5 ± 0.5	16.3 ± 0.4
\perp	0.96 ± 0.02	~ 20	17 ± 1	32.6 ± 0.8

According to Eqs. (4), both parallel and perpendicular MSRDS can also be compared with absolute MSDs obtained from Bragg diffraction. MSD values for CuCl at room temperature can be found in the literature. By averaging all the available values,⁷⁻¹⁰ we obtained that the MSDs in any direction of Cu and Cl atoms are $\langle u_{\text{any}}^2 \rangle_{\text{Cu}} = (5.6 \pm 0.4) \times 10^{-2} \text{ \AA}^2$ and $\langle u_{\text{any}}^2 \rangle_{\text{Cl}} = (2.8 \pm 0.3) \times 10^{-2} \text{ \AA}^2$, respectively. Due to the cubic symmetry, the atomic vibrations around equilibrium positions are isotropic: therefore according to Eqs. (5), $\langle u_{\parallel}^2 \rangle = \langle u_{\text{any}}^2 \rangle$ and $\langle u_{\perp}^2 \rangle = 2 \langle u_{\text{any}}^2 \rangle$ for both Cu and Cl atoms. Parallel and perpendicular MSRDS are compared with the uncorrelated MSDs in Fig. 8 and Table I.

The MSRDS, both parallel and perpendicular, cannot exceed lower and upper bounds, $\langle \Delta u^2 \rangle_{\text{low}}$ and $\langle \Delta u^2 \rangle_{\text{upp}}$, corresponding to relative displacements perfectly in phase and perfectly in opposition of phase, respectively. The upper and lower bounds can be evaluated from the uncorrelated MSDs.^{19,32} For both parallel and perpendicular relative motions of a pair of atoms 1 and 2 one has

$$\langle \Delta u^2 \rangle_{\text{low}} = \langle u_1^2 \rangle + \langle u_2^2 \rangle - 2(\langle u_1^2 \rangle \langle u_2^2 \rangle)^{1/2}, \quad (8a)$$

$$\langle \Delta u^2 \rangle_{\text{upp}} = \langle u_1^2 \rangle + \langle u_2^2 \rangle + 2(\langle u_1^2 \rangle \langle u_2^2 \rangle)^{1/2}. \quad (8b)$$

The upper and lower bounds have been calculated for CuCl at room temperature and are given in Table I. The parallel MSRD is much smaller than the sum of the uncorrelated MSDs, but larger than the lower bound: the relative motion of Cu and Cl atoms along the bond direction is characterized by a strong positive correlation, which is, however, not the maximum possible, as was instead the case for cuprites Cu_2O and Ag_2O .¹⁹ The perpendicular MSRD is slightly larger than the sum of the uncorrelated MSDs; this fact could indicate that the relative motion is slightly anticorrelated in the perpendicular directions, although it is difficult to quantitatively assess the reliability of the MSDs, measured at only one temperature, and of the perpendicular MSRD, whose value at 300 K has been obtained by extrapolating the Einstein model from experimental data limited to 100 K. One should also consider that, in view of the quite strong anharmonicity of CuCl, the probability distribution functions can deviate from a spherical towards a tetrahedral shape already at relatively low temperatures;¹⁰ as a consequence, in spite of the high symmetry of CuCl, the isotropy conditions (5) could be not rigorously valid. In any case it seems clear that, while the relative atomic motion retains a considerable degree of correlation in the parallel direction, it is almost uncorrelated in the plane perpendicular to the bond.

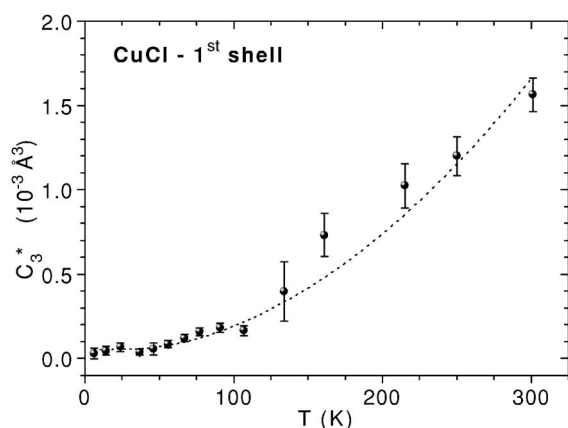


FIG. 9. Third cumulant (full circles); the dotted line is the best-fitting one-dimensional quantum theoretical model from Refs. 45 and 46. The best-fitting third order effective force constant is $k_3 = -1.234(6) \text{ eV}/\text{\AA}^3$. The 0 K value is $(2.9 \pm 0.9) \times 10^{-5} \text{ \AA}^3$.

C. Higher order cumulants

The introduction of higher order cumulants in EXAFS analysis was necessary to obtain highly accurate values of distance and mean square relative displacements. The temperature dependence of the third and fourth cumulants, shown in Figs. 9 and 10, respectively, is in agreement with the behavior expected according to one-dimensional quantum perturbative models^{45,46} (dotted lines). The good agreement with models represents a self-consistency test of data analysis and suggests that the shape of the effective pair potential is insensitive to temperature, as was found also for germanium²⁵ and copper.²⁴

The joint knowledge of the second and third cumulants is often considered equivalent to the knowledge of the first cumulant in order to measure the thermal expansion. This is certainly correct for a two-atomic molecule, but is highly questionable for many-atomic systems, where it amounts to attributing thermal expansion solely to the asymmetry of the effective pair potential. In Ref. 45, the thermal expansion due

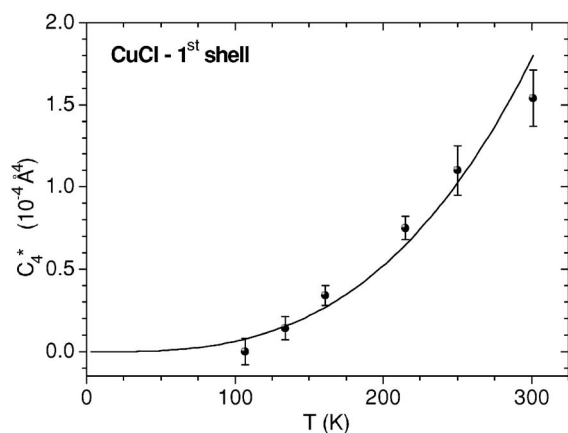


FIG. 10. Fourth cumulant (full circles); the dotted line is the best-fitting one-dimensional quantum theoretical model from Ref. 46 (see also Ref. 24). The best-fitting fourth order effective force constant is $k_4 \approx 2.7 \text{ eV}/\text{\AA}^4$. The 0 K value is $(0.0 \pm 0.2) \times 10^{-6} \text{ \AA}^4$.

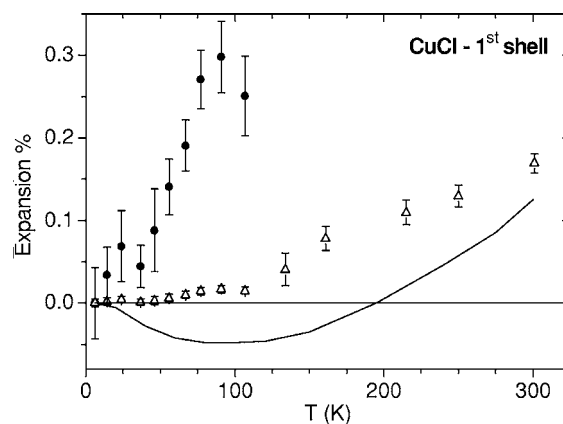


FIG. 11. The percent thermal expansion from the asymmetry of V_{eff} and calculated according to Ref. 45 (open triangles) is compared to the true bond expansion (closed circles) and to the crystallographic expansion (continuous line).

to the asymmetry of the potential has been calculated as $a = -3(k_3/k_0) C_2^*$, where $k_0 = \mu\omega^2$. It was, however, experimentally established that the quantity a does not correspond to the thermal expansion measured by the first EXAFS cumulant for either copper²⁴ or germanium.²⁵ This conclusion holds also for CuCl (Fig. 11): the thermal expansion measured by the quantity a is much weaker than the true bond expansion measured by δC_1^* .

VI. RESULTS: OUTER SHELLS

The analysis of outer shells could be done only in the low-temperature range (below about 100 K), at higher temperatures the corresponding signal is too weak (Fig. 4). The

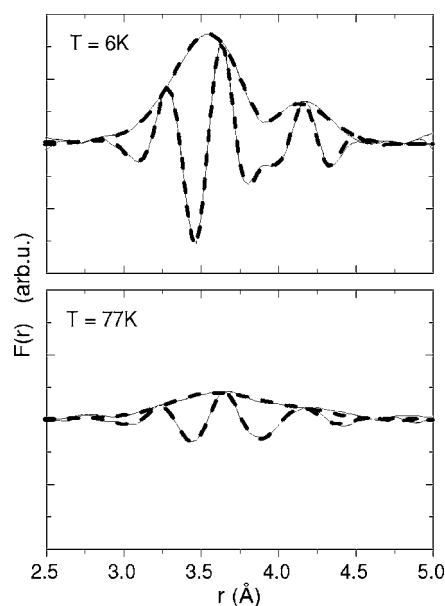


FIG. 12. Modulus and imaginary part of Fourier transform of the EXAFS signal (continuous lines) and best-fitting signals in the range $r = 2.7\text{--}4.6 \text{ \AA}$ (dash-boldd lines) at the temperatures of 6 K (upper panel) and 77 K (lower panel).

TABLE II. Scattering paths for CuCl within the third shell distance as calculated by FEFF8. For every path, the table contains: a path index, an approximate half-path length R , a percent importance factor with respect to the first shell SS path, the number of equivalent paths (degeneracy), the total number of legs, and a brief description.

Index	R (Å)	Percent importance	Degeneracy	Number of legs	Comment
1	2.34	100.00	4	2	SS 1st shell
2	3.82	71.54	12	2	SS 2nd shell
3	4.25	17.59	12	3	Triangular
4	4.25	35.79	24	3	Triangular
5	4.48	60.35	12	2	SS 3rd shell
6	4.68	8.19	4	4	Linear
7	4.68	11.72	12	4	Dogleg
8	4.68	4.14	12	4	Dogleg

r -space fitting range was between 2.7 and 4.6 Å (Fig. 12). All scattering paths calculated by FEFF8 within this distance range are listed in Table II and were included in the fitting procedure. Stable and meaningful results could be obtained only by a drastic reduction of the fitting parameters: (a) the thermal expansion of all SS and MS paths was described by a unique fitting coefficient ALPHA; (b) the second cumulants of the two SS paths (second and third shells) were considered as free parameters; and (c) the second cumulants of the (nonlinear) MS paths were constrained to a Debye model with $\theta_D=146$ K (Ref. 47). As for the first shell, the values of e_0 and S_0^2 were fixed to the average values ($e_0=0.08$ eV and $S_0^2=0.91$) obtained in a first trial analysis.

The absolute values of the parallel MSRDS, obtained by shifting the relative experimental values of the second cumulants according to the best fitting Einstein models, are shown in Fig. 13. Table III summarizes the corresponding Einstein frequencies.

The comparison of the $MSRD_{\parallel}$ obtained from EXAFS with the absolute MSDs measured by diffraction allows evaluating the effect of correlation parallel to the bond [Eq.

(4a)] on the different coordination shells. Since diffraction data are available only at room temperature (Refs. 7–10), the thermal behavior of EXAFS data for the second and third shells has been extrapolated up to 300 K according to the Einstein models. The parallel relative motion of the first (Cu-Cl) and second (Cu-Cu) shell atomic pairs is characterized by a quite strong correlation, the ratios $DCF/\sum MSD_i$ being 0.8 and 0.4, respectively. The third shell (Cu-Cl) motion appears instead uncorrelated.

The average thermal expansion of second and third shell distances obtained through the nonlinear best-fit procedure was found to be positive, although its percent values were considerably lower than the values measured for the nearest-neighbors distance. However, it should be emphasized here that the ALPHA parameter has a limited physical meaning, since it does not account for possible differences between the local expansions of the second and third shell; besides, the third cumulants were not included in the fitting procedure. In the case of copper,²⁴ reliable information on outer shells could be obtained only concerning the second cumulants.

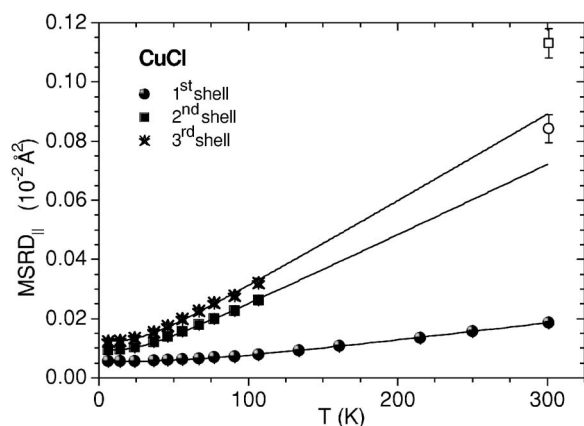


FIG. 13. Parallel MSRDS of the first three coordination shells of CuCl and best-fitting Einstein models (continuous lines). For comparison, the sum of uncorrelated parallel MSDs of the atomic pairs Cu+Cl (open circle) and Cu+Cu (open square) are also shown. See the text for discussion.

VII. DISCUSSION

The coefficients of thermal expansion measured by Bragg diffraction and by macroscopic dilatometric techniques are in principle equivalent. For a simple structure like zinc blende, where no internal coordinates are necessary, the expansion of the distance between average positions of any atomic pair is proportional to the expansion of the lattice parameter measured by Bragg diffraction. In CuCl, the distance between average positions of nearest neighbors copper and chlorine atoms undergoes negative expansion up to 100 K ($\alpha_{\min} \approx -0.8 \times 10^{-5} \text{ K}^{-1}$) and positive expansion above 100 K

TABLE III. Best fitting Einstein frequencies for the parallel MSRDS of the first three coordination shells of CuCl.

	1st shell	2nd shell	3rd shell
ν_E^{\parallel} (THz)	3.93(2)	1.665(8)	1.77(2)

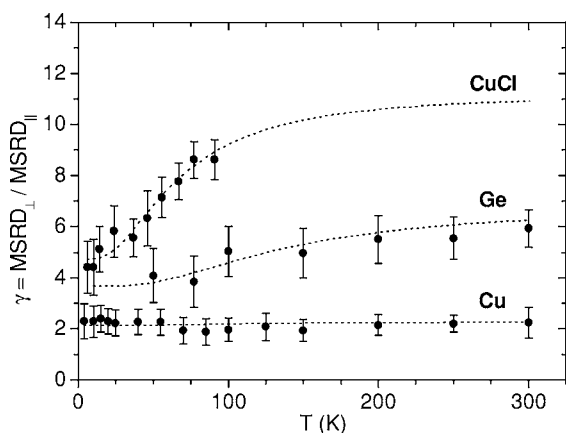


FIG. 14. Ratio γ between perpendicular and parallel MSRDs of CuCl (present work), germanium (Ref. 25), and copper (Ref. 24). The dotted lines are the ratio between the best-fitting Einstein models.

($\alpha_{\max} \approx +1 \times 10^{-5} \text{ K}^{-1}$), while the average distance measured by the first EXAFS cumulant undergoes a positive and stronger expansion at all temperatures ($\alpha_{\max} \approx +4.3 \times 10^{-5} \text{ K}^{-1}$, Fig. 7).

A positive first-shell expansion was found also in the NTE compounds Cu_2O and Ag_2O by EXAFS measurements¹⁹ and in quartz and $\text{Zn}(\text{CN})_2$ by total neutron scattering measurements.^{48,49} For the two isostructural compounds Cu_2O and Ag_2O , the system with the largest macroscopic NTE is characterized also by the largest first-shell positive expansion.

The difference between EXAFS and Bragg diffraction expansions is due to perpendicular vibrations [Eq. (1)]. In relatively open structures, one can reasonably expect that, when the perpendicular to parallel anisotropy of relative vibrations increases, the tension effect giving rise to NTE increases, but more room is also at the disposal of the nearest-neighbors bond for expanding under the influence of the stretching effect.

Concerning perpendicular vibrations, a further difference between Bragg diffraction and EXAFS has to be stressed. In many framework structures, linear A-B-A links are present, and anisotropic thermal factors are found by diffraction for the central atoms B: the vibrations perpendicular to the A-B-A direction are more intense than the parallel vibrations. In Cu_2O and Ag_2O , EXAFS measurements have revealed that the anisotropy of the *relative* displacement of Cu or Ag with respect to O is much stronger than the anisotropy of the *absolute* displacement of the Cu or Ag atoms. Besides, the anisotropy of relative vibrations, measured by the ratio $\gamma = \langle \Delta u_{\perp}^2 \rangle / \langle \Delta u_{\parallel}^2 \rangle$, is larger for Ag_2O , which has the stronger NTE.

In the case of the zinc-blende structure, the thermal factors measured by diffraction are isotropic, for symmetry reasons. It is reasonable to assume that a connection exists between NTE and anisotropy of *relative* vibrations, as measured by the ratio γ . The quantity γ is, to a good approximation, the ratio between two Einstein models, and, to the extent that the two Einstein frequencies are different, it is temperature dependent. For perfectly isotropic relative vibra-

tions, $\gamma=2$, independent of temperature. The thermal behavior of the first-shell γ for CuCl is shown in Fig. 14, where the results previously obtained for germanium²⁵ and copper²⁴ are shown for comparison. In the close-packed fcc structure of copper there is no negative expansion; the ratio γ is only slightly different from two, corresponding to a tiny anisotropy. In germanium, macroscopic NTE is observed, although restricted to a limited temperature range and anyway much weaker ($\alpha_{\min} \approx -0.07 \times 10^{-6} \text{ K}^{-1}$) (Ref. 50) than in CuCl. Correspondingly, the ratio γ is larger in germanium than in copper and larger in CuCl than in germanium. The asymptotic high-temperature values are $\gamma \approx 2.7, 6$, and 11 for copper, germanium, and CuCl, respectively.

To find a quantitative expression for the relationship between NTE and ratio γ is, however, far from trivial.²⁶ For the diamond and zinc-blende structures, NTE increases with increasing ionicity: Noncentral forces, stronger in crystals of weaker ionicity, reduce the tension effect by resisting vibrations transverse to bond direction, and as a consequence reduce the NTE.^{20,22} EXAFS measurements on tetrahedrally bonded systems with NTE and ionicity intermediate between Ge and CuCl, like CdTe and HgTe, could contribute to establish a quantitative relation between γ and NTE. Still more challenging is the comparison between different structures. In cuprites, asymptotic γ values of 6 and 22 were found for Cu_2O and Ag_2O , respectively. The difference is qualitatively consistent with the different NTE behavior of the two compounds. CuCl and Ag_2O have quite similar minimum values of NTE; the large difference in the γ values could be connected to the fact that in Ag_2O , contrary to CuCl, NTE persists up to the highest temperatures. The γ value is instead very similar in germanium and in Cu_2O , in spite of the very different NTE, suggesting that the relation between γ and NTE is somewhat structure dependent.

The balance between the effects of stretching and tension mechanisms, giving rise to the balance between negative and positive expansions, depends on the frequency distribution of normal modes, as well as on their eigenvectors and Grüneisen parameters. The Einstein frequencies, obtained from the best fit to the temperature dependence of the EXAFS MSRDs, can be compared to the calculated dispersion curves and phonon density of states (DOS) of CuCl. The calculated CuCl phonon DOS are characterized by three well-separated groups of frequencies:¹³ the transverse acoustic (TA) modes give rise to a narrow band below 1.4 THz, the longitudinal acoustic (LA) modes give rise to a Debye-like band extending up to 3.8 THz, while optical modes are distributed between 5 and 7.6 THz. In general, the EXAFS Einstein frequencies do not correspond with definite peaks in the phonon DOS.⁴⁴ However, the values of Einstein frequencies for the first-shell perpendicular and parallel MSRD of CuCl (1.66 and 3.93 THz, respectively), when compared with the calculated DOS, suggest that the low-energy TA modes play a more determinant role, for perpendicular relative motion, than the LA and optical modes.

Transverse acoustic modes have been often associated with NTE in diamond and zinc-blende structures: in the case of CuCl, it was shown, from *ab initio* calculations¹³ performed in the framework of the quasiharmonic approximation (QHA)⁵¹ for crystals, that the TA mode at zone boundary

points (X and L) have a negative Grüneisen parameter and therefore contribute to NTE. A negative Grüneisen parameter for TA modes at the zone boundary was found also in diamond-type crystals from the pressure dependence of the phonon frequencies.^{52–54}

VIII. CONCLUSIONS

The EXAFS structure at the K edge of copper in CuCl has been studied as a function of temperature, from 6 to 300 K, in order to gain a deeper insight into the local mechanisms of negative thermal expansion. The main results can be summarized as follows:

(a) While the distance between the average positions of copper and chlorine undergoes negative expansion below 100 K, the expansion of the Cu-Cl bond length is positive at all temperatures. The difference between EXAFS and Bragg diffraction expansions is due to relative vibrations perpendicular to the Cu-Cl bond.

(b) The relative thermal vibrations exhibit a marked perpendicular to parallel anisotropy, in contrast with the isotropy of the single atom absolute thermal factors. The relative anisotropy is reasonably connected to the tension mechanism responsible for NTE.

(c) A connection can be established between perpendicular MSRD and low-energy transverse acoustic modes, which

are known to be responsible for NTE in zinc-blende structures.

(d) The Cu-Cl bond thermal expansion cannot be obtained from the third cumulant. A similar result was found for the nearest-neighbor distances in copper and germanium.

(e) Accurate information on outer shells has been obtained concerning the parallel MSRD; the relative thermal motion parallel to the interatomic bond is largely correlated for the first and second shells, while it is practically uncorrelated for the third shell.

This work confirms the effectiveness of EXAFS for investigating NTE materials, thanks to the possibility of directly measuring the bond thermal expansion and, by comparison with Bragg diffraction, the anisotropy of relative thermal vibrations.

ACKNOWLEDGMENTS

We are grateful to C. Armellini, N. Afify, and R. Graziola for technical help. We acknowledge the European Synchrotron Radiation Facility (ESRF) for provision of synchrotron radiation facilities, as well as F. d'Acapito and the staff of the BM08-Gilda beamline for technical assistance. This work has been partially supported by the INFN project BM08-01-687. One of the authors, A.S., acknowledges the financial support of the Provincia Autonoma di Trento, through the LOTHEX project at IFN-CNR.

*Email address: paolo.fornasini@unitn.it

¹J. C. Phillips, *Rev. Mod. Phys.* **42**, 317 (1970).

²R. M. Martin, *Phys. Rev. B* **1**, 4005 (1970).

³R. C. Hanson, J. R. Hallberg, and C. Schwab, *Appl. Phys. Lett.* **21**, 490 (1972).

⁴J. N. Plendl, A. Hadni, J. Claudel, Y. Henninger, G. Morlot, P. Strimer, and L. C. Mansur, *Appl. Opt.* **5**, 397 (1966).

⁵J. N. Plendl and L. C. Mansur, *Appl. Opt.* **11**, 1194 (1972).

⁶Z. Vardeny, G. Gilat, and D. Moses, *Phys. Rev. B* **18**, 4487 (1978).

⁷M. Sakata, S. Hoshino, and J. Harada, *Acta Crystallogr., Sect. A: Cryst. Phys., Diffr., Theor. Gen. Crystallogr.* **30**, 655 (1974).

⁸J. Schreurs, M. H. Mueller, and L. H. Schwartz, *Acta Crystallogr., Sect. A: Cryst. Phys., Diffr., Theor. Gen. Crystallogr.* **32**, 618 (1976).

⁹V. Valvoda and J. Ječný, *Phys. Status Solidi A* **45**, 269 (1978).

¹⁰F. Altorfer, B. Graneli, P. Fischer, and W. Buhner, *J. Phys.: Condens. Matter* **6**, 9949 (1994).

¹¹S. Hull and D. A. Keen, *Phys. Rev. B* **50**, 5868 (1994).

¹²B. Prevot, B. Hennion, and B. Dorner, *J. Phys. C* **10**, 3999 (1977).

¹³Y. Ma, J. Tse, and D. Klug, *Phys. Rev. B* **67**, 140301(R) (2003).

¹⁴I. P. Kaminow and E. H. Turner, *Phys. Rev. B* **5**, 1564 (1972).

¹⁵H. F. Schaaake, Air Force Cambridge Research Laboratories Technical Report No. AFCRL-69-0538, 1969, quoted in Ref. 5 (unpublished).

¹⁶T. H. K. Barron, J. G. Collins, and G. K. White, *Adv. Phys.* **29**, 609 (1980).

¹⁷T. H. K. Barron, J. A. Birch, and G. K. White, *J. Phys. C* **10**, 1617 (1977).

¹⁸T. A. Mary, J. S. O. Evans, T. Vogt, and A. W. Sleight, *Science* **272**, 90 (1996).

¹⁹A. Sanson, F. Rocca, G. Dalba, P. Fornasini, R. Grisenti, M. Dapiaggi, and G. Artioli, *Phys. Rev. B* **73**, 214305 (2006).

²⁰R. E. Taylor *et al.*, in *CINDAS Data Series on Material Properties*, edited by C. Y. Ho (ASM International, Materials Park, OH, 1998), Vol. 1, Chap. 1, pp. 1–108.

²¹T. H. K. Barron and G. K. White, *Heat Capacity and Thermal Expansion at Low Temperatures* (Kluwer Academic/Plenum Publishers, New York, 1999).

²²G. D. Barrera, J. A. O. Bruno, T. H. K. Barron, and N. L. Allan, *J. Phys.: Condens. Matter* **17**, R217 (2005).

²³J. Tao and A. Sleight, *J. Solid State Chem.* **173**, 442 (2003).

²⁴P. Fornasini, S. a Beccara, G. Dalba, R. Grisenti, A. Sanson, M. Vaccari, and F. Rocca, *Phys. Rev. B* **70**, 174301 (2004).

²⁵G. Dalba, P. Fornasini, R. Grisenti, and J. Purans, *Phys. Rev. Lett.* **82**, 4240 (1999).

²⁶P. Fornasini, G. Dalba, R. Grisenti, J. Purans, M. Vaccari, F. Rocca, and A. Sanson, *Nucl. Instrum. Methods Phys. Res. B* **246**, 180 (2006).

²⁷D. Cao, F. Bridges, G. R. Kowach, and A. P. Ramirez, *Phys. Rev. B* **68**, 014303 (2003).

²⁸J. B. Boyce, T. M. Hayes, and J. C. Mikkelsen, Jr., *Solid State Commun.* **35**, 237 (1980).

²⁹J. B. Boyce, T. M. Hayes, and J. C. Mikkelsen, Jr., *Phys. Rev. B* **23**, 2876 (1981).

- ³⁰G. Bunker, Nucl. Instrum. Methods Phys. Res. **207**, 437 (1983).
- ³¹P. Fornasini, F. Monti, and A. Sanson, J. Synchrotron Radiat. **8**, 1214 (2001).
- ³²W. R. Busing and H. A. Levy, Acta Crystallogr. **17**, 142 (1964).
- ³³G. Dalba, P. Fornasini, R. Gotter, and F. Rocca, Phys. Rev. B **52**, 149 (1995).
- ³⁴G. Beni and P. M. Platzman, Phys. Rev. B **14**, 1514 (1976).
- ³⁵A. A. Maradudin, E. W. Montroll, G. H. Weiss, and I. P. Ipatova, *Theory of Lattice Dynamics in the Harmonic Approximation* (Academic Press, New York, 1971).
- ³⁶B. T. M. Willis and A. W. Pryor, *Thermal Vibrations in Crystallography* (Cambridge University Press, Cambridge, England, 1975).
- ³⁷O. H. Nielsen and W. Weber, J. Phys. C **13**, 2449 (1980).
- ³⁸S. Kraft, J. Stümpel, P. Becker, and U. Kuetgens, Rev. Sci. Instrum. **67**, 681 (1996).
- ³⁹J. M. Tranquada and R. Ingalls, Phys. Rev. B **28**, 3520 (1983).
- ⁴⁰A. L. Ankudinov, B. Ravel, J. J. Rehr, and S. D. Conradson, Phys. Rev. B **58**, 7565 (1998).
- ⁴¹M. Newville, B. Ravel, J. J. Rehr, E. Stern, and Y. Yacoby, Physica B **208-209**, 154 (1995).
- ⁴²J. Freund, R. Ingalls, and E. D. Crozier, Phys. Rev. B **39**, 12537 (1989).
- ⁴³M. Vaccari, Ph.D. thesis, University of Trento (Italy), 2006.
- ⁴⁴M. Vaccari and P. Fornasini, J. Synchrotron Radiat. **13**, 321 (2006).
- ⁴⁵A. I. Frenkel and J. J. Rehr, Phys. Rev. B **48**, 585 (1993).
- ⁴⁶T. Yokoyama, J. Synchrotron Radiat. **6**, 323 (1999).
- ⁴⁷R. Banerjee and Y. P. Varshni, Solid State Commun. **9**, 2115 (1971).
- ⁴⁸M. G. Tucker, M. T. Dove, and D. A. Keen, J. Phys.: Condens. Matter **12**, L425 (2000).
- ⁴⁹K. W. Chapman, P. J. Chupas, and C. J. Kepert, J. Am. Chem. Soc. **127**, 15630 (2005).
- ⁵⁰T. F. Smith and G. K. White, J. Phys. C **8**, 2031 (1975).
- ⁵¹G. Leibfried and W. Ludwig, Solid State Phys. **12**, 275 (1961).
- ⁵²R. T. Payne, Phys. Rev. Lett. **13**, 53 (1964).
- ⁵³W. Richter, J. B. Renucci, and M. Cardona, Solid State Commun. **16**, 131 (1975).
- ⁵⁴B. A. Weinstein and G. J. Piermarini, Phys. Rev. B **12**, 1172 (1975).